

Mode structure of a quantum cascade laser

A. A. Bogdanov* and R. A. Suris†

A. F. Ioffe Physico-Technical Institute, 26 Polytekhnicheskaya, St. Petersburg 194021, Russian Federation

(Received 16 June 2010; published 25 March 2011)

We analyze the mode structure of a quantum cascade laser (QCL) cavity considering the surface plasmon-polariton modes and familiar modes of hollow resonator jointly, within a single model. We present a comprehensive mode structure analysis of the laser cavity, varying its geometric parameters and free electron concentration inside cavity layers within a wide range. Our analysis covers, in particular, the cases of metal-insulator-metal and insulator-metal-insulator waveguides. We discuss the phenomenon of negative dispersion for eigenmodes in detail and explain the nature of this phenomenon. We specify a waveguide parameters domain in which negative dispersion exists. The mode structure of QCL cavity is considered in the case of the anisotropic electrical properties of the waveguide materials. We show that anisotropy of the waveguide core results in propagation of Langmuir modes that are degenerated in the case of the isotropic core. Comparative analysis of optical losses due to free carrier absorption is presented for different modes within the frequency range from terahertz to ultraviolet frequencies.

DOI: [10.1103/PhysRevB.83.125316](https://doi.org/10.1103/PhysRevB.83.125316)

PACS number(s): 42.79.Gn, 71.36.+c, 73.20.Mf, 73.40.Rw

I. INTRODUCTION

An active region of quantum cascade laser (QCL) is a superlattice (SL) of tunnel-coupled quantum wells located at regular intervals. The idea of SL application to light amplification was first put forward in 1971.¹ However, it was realized only two decades later, in 1994.²

The first QCLs operated within the midinfrared region. To extend the lasing range toward the terahertz (THz) region (1–10 THz, 30–300 μm), it is necessary to overcome some fundamental problems. One of them is how to minimize free carrier absorption (FCA). These losses increase with wavelength roughly as $\sim\lambda^2$ (see, e.g., Refs. 3 and 4). To reduce them, one can increase the optical confinement factor or suppress the electron motion along the layers of the active region. The latter can be achieved in a quantum dot cascade laser.^{5–7}

The maximal operating wavelength of a laser with conducting waveguide faces is about double the thickness of the waveguide.⁸ Therefore, a QCL operating at THz frequencies should be rather thick. It is a problem to fabricate QCL structures thicker than 10–15 μm using standard techniques, such as molecular beam epitaxy metal-organic chemical vapor deposition.⁴

Overcoming the problem of the maximal operating wavelength of QCLs is possible by means of exploiting surface plasmon polariton (SPP) modes and surface plasmon waveguides.^{9–11} Just such a solution was used to fabricate the first THz QCL¹² and first THz QCL operating at room temperature.¹³

The SPP propagates along the interface between two media if the signs of their dielectric functions are opposite.^{14,15} This condition can be fulfilled, for example, for metal-dielectric structures, for heavily and lightly doped semiconductors, and for metal-semiconductor structures. The SPP field is localized near the interface. It represents two tails exponentially decreasing depthward. The SPP properties are well documented (see, e.g., Refs. 14–21). A planar waveguide has two interfaces, and SPPs can be localized at both of them. The

interference of two SPPs results in the formation of SPP modes (surface modes).

The other kind of eigenmodes is formed due to total reflection of electromagnetic waves from the waveguide walls. We call this kind of eigenmode a volume mode,²² in contrast to a surface mode. The problem of electromagnetic wave interaction with free carriers of the medium has been studied for more than a century.^{16,23,24} Seemingly, the first works devoted to properties of waveguides taking into account the free carriers of the materials are Refs. 25–28. Today investigations in this area are extremely relevant due to the development of subwavelength optics and compact photonic devices.^{15,29–31}

Under some conditions specified below eigenmodes have a negative dispersion. Such behavior was discussed in Refs. 26 and 28 for surface modes. Here we show that negative dispersion can appear not only for surface modes but also for volume modes. We explain the nature of negative dispersion and obtain the critical waveguide parameters at which this phenomenon can be observed.

In this paper we present an in-depth and comprehensive mode structure analysis of the QCL cavity. We start the analysis with a model description of the QCL waveguide (Sec. II) and a fundamental equation describing the field distribution and dispersion law for the eigenmodes in the cavity (Sec. III). In Sec. IV we analyze the mode structure and eigenmode field distributions in a QCL waveguide with an isotropic core. The analysis covers the cases of arbitrary waveguide core thickness and arbitrary free electron concentrations in the cladding layers and core. At the end of Sec. IV we classify mode structures of waveguides depending on the waveguide core thickness and doping level of the materials. In Sec. V we discuss in detail the phenomenon of negative dispersion for the volume and surface modes. In Sec. VI we analyze the mode structure of a QCL waveguide with an anisotropic core. We show that anisotropy results in propagation of Langmuir modes, which are degenerated in the case of an isotropic core. Cases of different ratios between injector thickness and active section

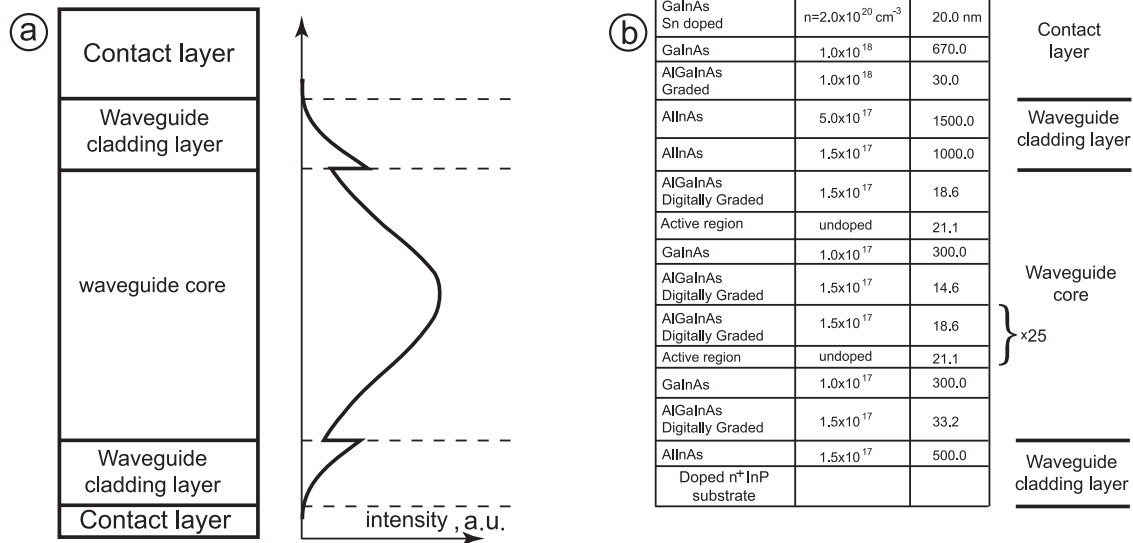


FIG. 1. (a) Schematic construction of the QCL. Approximate distribution of mode intensity in the QCL cavity. The jumps of the field intensity are caused by the difference between dielectric functions of the waveguide core and cladding layers. (b) Schematic cross section of the first QCL.²

thickness are analyzed. Section VII provides an FCA analysis of the volume and surface modes. We analyze FCA in the cases of metal and semiconductor cladding layers. Losses due to FCA for the volume and surface modes are compared at different frequencies.

II. MODEL

The QCL has a complicated multilayer structure [Fig. 1(b)], but it is possible to distinguish three types of layers—(i) contact layers, (ii) cladding layers, and (iii) core layers [Fig. 1(a)—that contain a stack of amplification cascades (active region). Due to the high free electron concentration in the cladding layers, the main part of the mode intensity is contained in the waveguide core layers [Fig. 1(a)]. Therefore, contact layers do not affect the mode structure and we ignore them in our model. The exception to this approach is the case of a waveguide with the contacts playing a role in the cladding layers.^{10,11} This case is considered in Sec. IV A and Sec. VII B.

A simplified model of a QCL waveguide is shown in Fig. 2. It is a symmetric planar waveguide consisting of a waveguide core of finite thickness that is surrounded by two cladding layers of identical materials and infinite thickness. Consideration of an asymmetric waveguide is given in Ref. 32.

Media numeration and coordinates are shown in Fig. 2. Usually lateral dimensions of the QCL cavity far exceed its thickness. Therefore, we consider the waveguide to be infinite in the y and z directions and we neglect the y dependence of waveguide fields. The effect of finiteness lateral dimensions of the QCL cavity on the parameters of QCL is discussed in Ref. 33.

In our model we describe the dielectric function of cladding layers within the Drude-Lorentz approximation:³⁴

$$\varepsilon_s(\omega) = \varepsilon_s^\infty \left(1 - \frac{\Omega_s^2}{\omega(\omega + i\gamma_s)} \right). \quad (1)$$

The s index is the medium number ($s = 1, 2, 3$) (see Fig. 2), ε_s^∞ is the material permittivity at $\omega \rightarrow \infty$, and γ_s is the inverse relaxation time, which is responsible for conductivity and energy dissipation due to FCA. Ω_s is the material plasma frequency, which is given by the expression⁸

$$\Omega_s = \sqrt{\frac{4\pi n_s e^2}{m_s^* \varepsilon_s^\infty}}, \quad (2)$$

where n_s is the concentration of free electrons and m_s^* is their effective mass.

Amplification cascades built in the waveguide core consist of alternate SL sections: active sections and injector sections.⁴ Therefore, the dielectric function of the waveguide core should be regarded as a tensor. We consider further two extreme cases.

(1) The active and injector sections occupy a small part of the waveguide core. So we can neglect the waveguide core anisotropy and expression (1) is correct for $s = 2$.

(2) The active and injector sections occupy a considerable part of the waveguide core. So we should consider the dielectric function of the waveguide core as a tensor with three nonzero

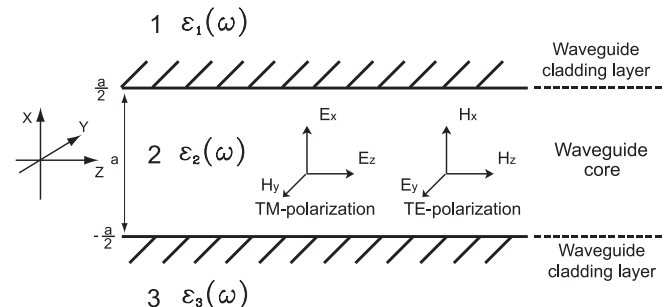


FIG. 2. Reductive QCL model. A symmetric planar waveguide.

components:

$$\widehat{\varepsilon}_2(\omega) = \begin{pmatrix} \varepsilon_{2xx}(\omega) & 0 & 0 \\ 0 & \varepsilon_{2yy}(\omega) & 0 \\ 0 & 0 & \varepsilon_{2zz}(\omega) \end{pmatrix}. \quad (3)$$

The components ε_{2zz} and ε_{2yy} are identical because the SL properties are supposed to be identical in the directions of the y and z axes. So, we can assign $\varepsilon_{2zz} = \varepsilon_{2yy} = \varepsilon_{||}$ and $\varepsilon_{2xx} = \varepsilon_{\perp}$. We discuss the frequency dependence of $\varepsilon_{||}$ and ε_{\perp} in Sec. VI.

III. DISPERSION LAW OF CAVITY EIGENMODES

We seek solution of Maxwell's equations in the form of a traveling wave propagating in the z direction (Fig. 2) and localized in the x direction. Then both the electric and the magnetic fields depend on the coordinate z and time t through a factor $\exp(ik_z z - i\omega t)$, where k_z is the sought function of ω that determines the dispersion law of eigenmodes.

Induced transitions in QCL are stimulated only by the electric field component normal to the SL layers.¹ In our case, it is E_x (see Fig. 2). This field component is nonzero only for TM modes. Therefore, we consider the modes of TM polarization only. An analysis of TE modes in the waveguide under consideration is presented in Ref. 35.

The Z component of the electric field, $E_{sz}(x)$, satisfies the Helmholtz equation for anisotropic media:

$$\frac{d^2}{dx^2} E_{sz} + \frac{\varepsilon_{s||}}{\varepsilon_{s\perp}} \left(\frac{\varepsilon_{s\perp} \omega^2}{c^2} - k_z^2 \right) E_{sz} = 0. \quad (4)$$

where $\varepsilon_{s\perp}$ and $\varepsilon_{s||}$ are the x - and z -tensor components of the dielectric function. We seek the solutions of this equation that meet the following boundary conditions:

$$\lim_{x \rightarrow \infty} E_{1z}(x) \rightarrow 0, \quad \lim_{x \rightarrow -\infty} E_{3z}(x) \rightarrow 0. \quad (5)$$

The waveguide symmetry allows division of the modes into two types.

(1) *Symmetric modes*: $E_x(x)$ is an even function and $E_z(x)$ is an odd function.

(2) *Antisymmetric modes*: $E_x(x)$ is an odd function and $E_z(x)$ is an even function.

Solution of the Helmholtz equation (4) for symmetric and antisymmetric modes can be presented as follows.

For the symmetric mode:

$$\begin{aligned} E_{1z} &= E_{1z}^o \exp\left(\left(\frac{a}{2} - x\right)\kappa\right), \\ E_{2z} &= E_{1z}^o \sin(Kx), \\ E_{3z} &= -E_{1z}^o \exp\left(\left(x + \frac{a}{2}\right)\kappa\right). \end{aligned}$$

For the antisymmetric mode:

$$\begin{aligned} E_{1z} &= E_{1z}^o \exp\left(\left(\frac{a}{2} - x\right)\kappa\right), \\ E_{2z} &= E_{1z}^o \cos(Kx), \\ E_{3z} &= E_{1z}^o \exp\left(\left(x + \frac{a}{2}\right)\kappa\right). \end{aligned}$$

In the above sets of equations, $\kappa = \sqrt{k_z^2 - \frac{\varepsilon_{s\perp} \omega^2}{c^2}}$ is the inverse penetration depth inside the cladding layers and $K = \sqrt{\frac{\varepsilon_{||}}{\varepsilon_{\perp}} \left(\frac{\varepsilon_{\perp} \omega^2}{c^2} - k_z^2 \right)}$ is the normal component of the wave vector in the waveguide core (Fig. 2).

The components of electric and magnetic fields (E_x and H_y) can be expressed in terms of E_z :

$$H_{sy} = i \frac{\varepsilon_{s\perp} \omega}{c \left(\frac{\varepsilon_{s\perp} \omega^2}{c^2} - k_z^2 \right)} \frac{d}{dx} E_{sz}, \quad (6)$$

$$E_{sx} = i \frac{k_z}{\left(\frac{\varepsilon_{s\perp} \omega^2}{c^2} - k_z^2 \right)} \frac{d}{dx} E_{sz}. \quad (7)$$

Equality of electric and magnetic field tangential component on the waveguide interfaces yields an implicit functional relationship between ω and k_z . For the symmetric modes, it is

$$\cot\left(\frac{\pi}{2} \widetilde{K}\right) = \frac{\varepsilon_{\perp}}{\varepsilon_{||}} \frac{\widetilde{K}}{\widetilde{\kappa}}. \quad (8)$$

And for antisymmetric modes, it is

$$\tan\left(\frac{\pi}{2} \widetilde{K}\right) = -\frac{\varepsilon_{\perp}}{\varepsilon_{||}} \frac{\widetilde{K}}{\widetilde{\kappa}}. \quad (9)$$

Here we use dimensionless quantities:

$$\begin{aligned} \widetilde{\omega} &= \omega \frac{\sqrt{\varepsilon_{2\perp}^{\infty}} a}{\pi c}, \quad \widetilde{\Omega}_s = \Omega_s \frac{\sqrt{\varepsilon_{2\perp}^{\infty}} a}{\pi c}, \quad \widetilde{\gamma}_s = \gamma_s \frac{\sqrt{\varepsilon_{2\perp}^{\infty}} a}{\pi c}, \\ \widetilde{k}_z &= k_z \frac{a}{\pi}, \quad \widetilde{K} = K \frac{a}{\pi}, \quad \widetilde{\kappa} = \kappa \frac{a}{\pi}. \end{aligned}$$

In terms of dimensionless quantities, Eqs. (8) and (9) do not depend on the waveguide thickness a and permit scaling. This means that the mode structure of a thick waveguide with heavily doped cladding layers is the same as the mode structure of a thin waveguide with heavily doped cladding layers.

IV. MODE STRUCTURE OF A WAVEGUIDE WITH AN ISOTROPIC CORE

A. Thick waveguide with an undoped core

In this section we consider the simplest case of nondissipative ($\gamma_1 = \gamma_2 = \gamma_3 = 0$) and isotropic materials of waveguide core and cladding layers. For the sake of simplicity, in what follows we set $\varepsilon_1^{\infty} = \varepsilon_2^{\infty} = \varepsilon_3^{\infty} = \varepsilon^{\infty}$. The latter assumption is true enough because $\varepsilon^{\infty} \sim 10$ –12 for the materials used for QCL fabrication. Sometimes the material of waveguide cladding layers is a metal, especially gold³⁶ or copper,^{37,38} with $\varepsilon^{\infty} \sim 5$ (see, e.g., Ref. 39).

There are only two dimensionless parameters that we can vary: $\widetilde{\Omega}_1$ and $\widetilde{\Omega}_2$. In this section we neglect free carriers inside the waveguide core and set $\widetilde{\Omega}_2 = 0$.

The thickness of the waveguide core usually lies in the range from^{2,40} 2 to 15 μm . Keeping in mind the scalability of the problem, for the sake of clarity, let us consider a QCL with an 8- μm -thick undoped ($n_2 = 0 \text{ cm}^{-3}$) GaAs waveguide core and heavily doped ($n_{1,3} = 5 \times 10^{18} \text{ cm}^{-3}$) GaAs cladding layers. The effective mass of an electron in GaAs is $m^* = 0.07m_e$, and $\varepsilon^{\infty} = 11.6$. According to Eq. (2), we have the plasma frequency of cladding layers $\Omega_1 = 1.4 \times 10^{14} \text{ s}^{-1}$. Using dimensionless quantities, we have $\widetilde{\Omega}_1 = 4.1$.

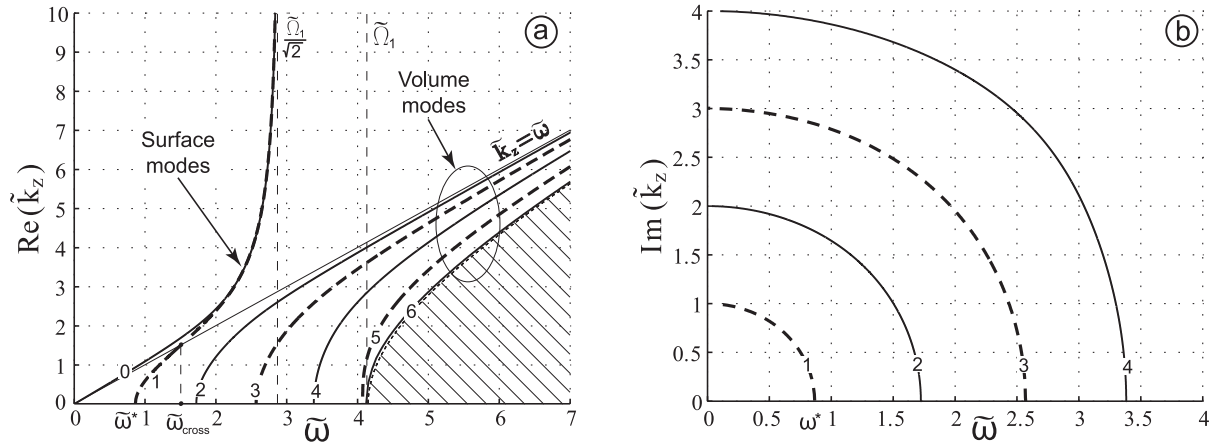


FIG. 3. (a) $\text{Re}(\tilde{k}_z)$ versus $\tilde{\omega}$. (b) $\text{Im}(\tilde{k}_z)$ versus $\tilde{\omega}$. Waveguide parameters are $\tilde{\Omega}_1 = 4.1$ and $\tilde{\Omega}_2 = 0$. Symmetric modes are represented by solid curves; antisymmetric modes, by dashed curves.

Equations (8) and (9) yield an implicit dependence of the longitudinal wave vector component, \tilde{k}_z , on the wave frequency, $\tilde{\omega}$, that is, the dispersion law for the eigenmodes. We can consider $\tilde{\omega}$ to be a real number and then \tilde{k}_z is a complex number. The imaginary part of \tilde{k}_z [$\text{Im}(\tilde{k}_z)$] is a coefficient of wave amplitude decrease. If there are no optical losses ($\gamma_1 = \gamma_2 = \gamma_3 = 0$), then wave attenuation is possible only within the spectral gaps of the cavity.

Numerical solutions of Eqs. (8) and (9) subjected to boundary conditions (5) are shown in Figs. 3(a) and 3(b). The electric and magnetic fields in the hatched area do not meet the boundary conditions (5). The equation for the hatched-area boundary is $\sqrt{k_z^2 - \varepsilon_1(\tilde{\omega})\tilde{\omega}^2} = 0$.

Dispersion curves of the first two modes (0 and 1) qualitatively differ from the rest. These are SPP modes¹⁴ or just surface modes. For them \tilde{k}_z increases infinitely as $\tilde{\omega} \rightarrow \frac{\tilde{\Omega}_1}{\sqrt{2}}$. The frequency $\tilde{\Omega}_{\text{sp}} = \frac{\tilde{\Omega}_1}{\sqrt{2}}$ is the surface plasmon frequency.¹⁴

The spatial distribution of the electric field component [$E_z(x)$] for them at $\tilde{\omega}$ close to $\tilde{\Omega}_{\text{sp}}$ is shown in Fig. 4(a). One can see that the fields of SPP modes are localized near the waveguide interfaces. Thus, SPP modes represent two independent surface waves at $\tilde{\omega} \rightarrow \tilde{\Omega}_{\text{sp}}$ [see Fig. 4(b)].

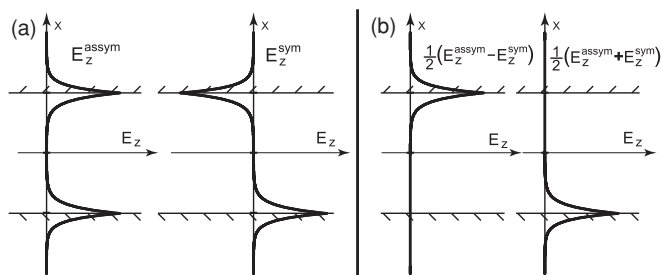


FIG. 4. Spatial distribution of the electric field z component [$E_z(x)$] for the SPP modes inside a waveguide at $\tilde{\omega} = 2.7$. Waveguide parameters are $\tilde{\Omega}_1 = 4.1$, $\tilde{\Omega}_2 = 0$. The surface plasmon frequency, $\tilde{\Omega}_{\text{sp}}$, is 2.9. Owing to the small overlapping of SPP tails, the SPP field can be considered either as (a) symmetric and antisymmetric modes or as (b) two independent SPPs.

The frequency cutoff for the symmetric SPP mode is 0 [Fig. 3(a)] and this mode can propagate at arbitrarily low frequencies. This allows us to use the symmetric SPP mode for fabrication of THz QCLs.

The volume modes are outlined by an ellipse in Fig. 3(a). Properties of these modes are well studied in the theory of a hollow metallic waveguide.^{8,41} We should note that at an arbitrary value of $\tilde{\Omega}_1$ there is always one volume mode with a frequency cutoff exactly equal to $\tilde{\Omega}_1$ [see Fig. 3(a)].

The spatial distribution of the electric field [$E_z(x)$] for the volume modes is shown in Fig. 5. One can see that the higher the frequency cutoff of the volume mode, the greater the penetration depth of this mode inside the cladding layers. The wave is mainly absorbed inside cladding layers. Therefore, it is quite reasonable to assume that FCA is larger for the modes with higher frequency cutoffs. The results of numerical analysis given in Sec. VII confirm this supposition.

It follows from Eqs. (8) and (9) that the number of eigenmodes N is finite. It depends on the dimensionless plasma frequency of the cladding layers only:

$$N = \left[\frac{\tilde{\Omega}_1}{2} \right] + \left[\frac{\tilde{\Omega}_1 + 1}{2} \right] + 3. \quad (10)$$

The brackets indicate the integer part of the number. So the number of waveguide eigenmodes increases with the thickness of the waveguide core and plasma frequency of cladding layers. At arbitrary $\tilde{\Omega}_1$ the waveguide always has at least three modes (two surface modes and one volume mode).

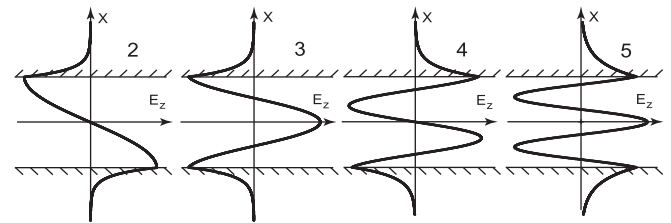


FIG. 5. Distribution of the electric field z component [$E_z(x)$] for the volume modes shown in Fig. 3(a). The field distribution is calculated for $\tilde{\omega} = 5$. Here the mode indexes correspond to the mode indexes in Fig. 3(a).

Here, it is reasonable to draw an analogy to the problem of localized states of an electron in a symmetric potential well. There is at least one localized state in a symmetric potential well of arbitrary shallow depth. The localized states of an electron might not exist in an asymmetric shallow potential well. Thus, the localized state of an electron in the potential well is unstable against symmetry breakdown of the well.⁴² In the waveguide we have a similar situation. The volume modes in a thin waveguide or in a waveguide with lightly doped cladding layers are unstable against symmetry breakdown of the waveguide design. In contrast to volume modes, surface modes are stable against symmetry breakdown of the waveguide design.³²

Let us analyze the mode structure of the waveguide and field distribution of eigenmodes depending on $\tilde{\Omega}_1$. We start with the case of high values of $\tilde{\Omega}_1$:

$$\tilde{\Omega}_1 \rightarrow \infty. \quad (11)$$

This case corresponds to a waveguide with perfectly conducting cladding layers. Therefore, there is no field inside the cladding layers and the wave penetration depth is 0. It follows from Eq. (10) that the mode number N is infinite. The dispersion characteristics of the volume mode coincide with the dispersion characteristics of a hollow waveguide with perfectly conducting faces.⁸

If $\tilde{\Omega}_1 \rightarrow \infty$, then the following relations are fulfilled for the symmetric surface mode:

$$\frac{E_{2z}}{E_{2x}} \sim \frac{1}{\tilde{\Omega}_1^{1/2}} \rightarrow 0; \quad (12)$$

$$\frac{E_{1z}}{E_{2x}} \approx \frac{E_{3z}}{E_{2x}} \sim \exp(-\tilde{\Omega}_1) \rightarrow 0; \quad (13)$$

$$\frac{E_{1x}}{E_{2x}} \approx \frac{E_{3x}}{E_{2x}} \sim \exp(-\tilde{\Omega}_1) \rightarrow 0. \quad (14)$$

Relation (12) means that the symmetric surface mode becomes transversal. Relations (13) and (14) mean that the wave is absolutely confined in the waveguide core. The dispersion characteristic of the symmetric surface mode tends to the dispersion characteristic of light inside the waveguide core [$\tilde{\omega} = \tilde{k}_z$; see Fig. 3(a)]. Modes with the above-named properties are called principal modes⁸ or TEM modes.⁴³ Propagation of these modes is possible if the waveguide cross section is a bi- or multiply connected domain. The waveguide cross section is the biconnected domain because the planar waveguide faces are separated by the waveguide core. Therefore, at limit (11) the symmetric surface mode transforms to the TEM mode of a symmetric planar waveguide with perfectly conducting walls.

At a high dimensionless plasma frequency of cladding layers ($\tilde{\Omega}_1 \gg 1$), the symmetric surface mode has three essential advantages over the other modes. The first is that there is no frequency cutoff. The second is that this mode is almost localized inside the waveguide core and so there is no significant FCA in the cladding layers. The third is that this mode is nearly transversal ($E_z \approx 0, E_x \neq 0$). So the electric field does not stimulate energy dissipation due to electron motion parallel to the SL layers and stimulates a laser transition only.

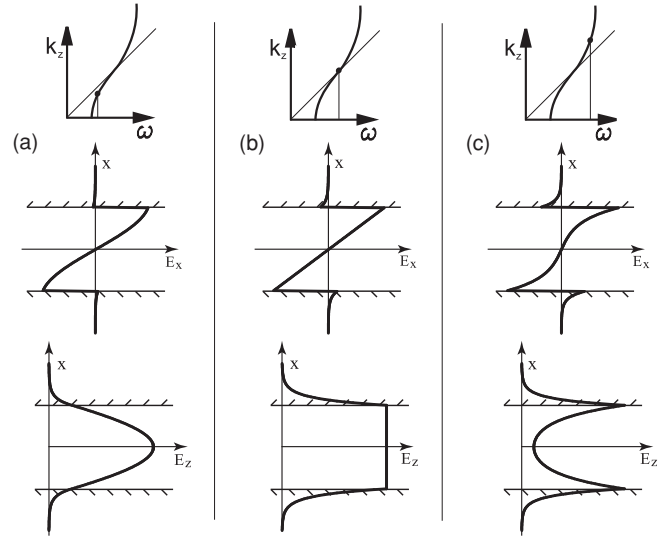


FIG. 6. Electric field distribution [$E_x(x)$ and $E_z(x)$] for the antisymmetric surface mode at (a) $\tilde{\omega} < \tilde{\omega}_{\text{cross}}$, (b) $\tilde{\omega} = \tilde{\omega}_{\text{cross}}$, and (c) $\tilde{\omega} > \tilde{\omega}_{\text{cross}}$.

The dispersion curve of the antisymmetric surface mode cuts the dispersion curve of light ($\tilde{\omega} = \tilde{k}_z$) at the frequency $\tilde{\omega}_{\text{cross}}$ [see Fig. 3(a)]:

$$\tilde{\omega}_{\text{cross}} = \frac{\tilde{\Omega}_1}{\sqrt{\frac{\pi}{2}\tilde{\Omega}_1 + 1}}. \quad (15)$$

The field distribution has a qualitative change at $\tilde{\omega}_{\text{cross}}$ (Fig. 6). At $\tilde{\omega} < \tilde{\omega}_{\text{cross}}$ the field distribution is similar to that of the first hollow metallic waveguide mode, that is, the first volume mode. At $\tilde{\omega} > \tilde{\omega}_{\text{cross}}$, the wave represents two overlapping SPPs. So the antisymmetric surface mode owns the volume and surface mode properties depending on $\tilde{\omega}$.

It follows from (15) that under condition (11), $\tilde{\omega}_{\text{cross}} \rightarrow \infty$. Therefore, under condition (11) the antisymmetric surface mode transforms to the first hollow metallic waveguide mode.

B. Thin waveguide

Above we have analyzed the waveguide mode structure at $\tilde{\Omega}_1 \gg 1$. In this section we consider the waveguide mode structure at a small value of $\tilde{\Omega}_1$ ($\tilde{\Omega}_1 \lesssim 1$ and $\tilde{\Omega}_1 \ll 1$).

According to Eq. (10) there are only three modes $\tilde{\Omega}_1 < 1$. The mode structure for this case is shown in Fig. 7(a). In the case of $\tilde{\Omega}_1 \ll 1$ the dispersion characteristic for the antisymmetric surface mode is ambiguous [see Fig. 7(b)]. Therefore, there is a frequency region with negative dispersion. The signs of the phase and group wave velocity are opposite within this frequency region.

The nonambiguity of the dispersion characteristic of the antisymmetric surface mode breaks at the plasma frequency $\tilde{\Omega}_1^*$. The value of $\tilde{\Omega}_1^*$ can be obtained from Eq. (9) with the side condition $\frac{dk_z}{d\omega}|_{\tilde{\omega}=\tilde{\omega}^*} = \infty$ at $\tilde{\Omega}_1 = \tilde{\Omega}_1^*$. Numerical computation yields $\tilde{\Omega}_1^* = 0.840$.

For example, the negative dispersion in a waveguide with heavily doped GaAs ($n_{1,3} = 5 \times 10^{18}$ 1/cm³) cladding layers and an undoped core can be observed if the core thickness is lower than 3.6 μm . In a planar metallic waveguide

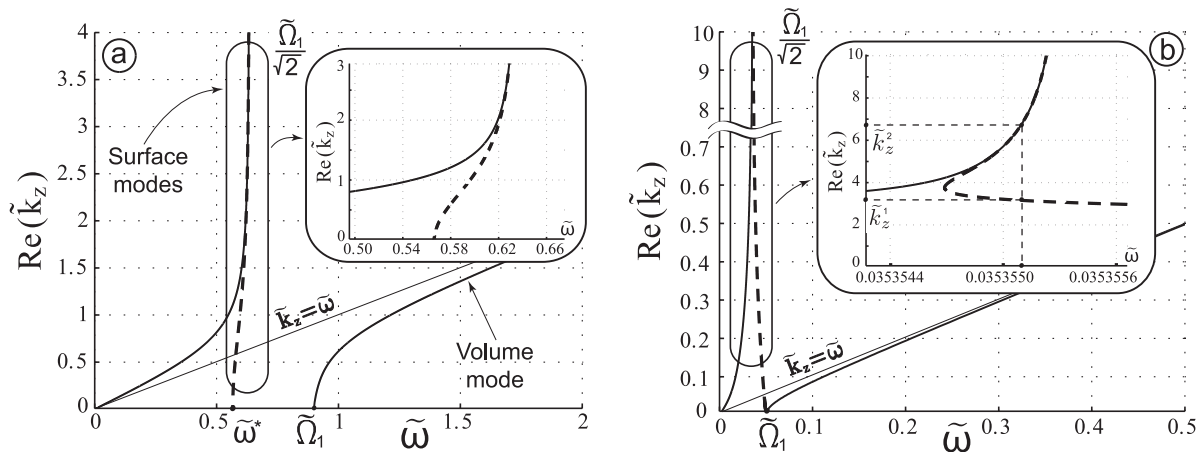


FIG. 7. $\text{Re}(\tilde{k}_z)$ versus $\tilde{\omega}$. (a) Waveguide parameters are $\tilde{\Omega}_1 = 0.9$ and $\tilde{\Omega}_2 = 0$. (b) Waveguide parameters are $\tilde{\Omega}_1 = 0.05$ and $\tilde{\Omega}_2 = 0$. Symmetric modes are represented by solid curves; antisymmetric modes, by dashed curves.

($n_{1,3} \sim 10^{22}$ 1/cm³) the negative dispersion can be observed experimentally if the core thickness is several nanometers or less.¹⁸

C. Free electrons in a waveguide core

Up to now, we have neglected free electrons in the waveguide core and assumed that $\tilde{\Omega}_2 = 0$. Actually, the waveguide core layers are doped [Fig. 1(b)]. Here we consider a waveguide with the same parameters as in Sec. IV A but with a doped core ($n_2 = 3.5 \times 10^{17}$ 1/cm³). Thus, the dimensionless waveguide parameters are $\tilde{\Omega}_1 = 4.1$ and $\tilde{\Omega}_2 = 1.1$.

The mode structure of such a waveguide is presented in Fig. 8. Taking into account free electrons in the waveguide core results in a qualitative change in the dispersion curve of the symmetric surface mode only. Now this mode has a frequency cutoff in contrast to the case of the undoped waveguide core ($\tilde{\Omega}_2 = 0$). In the case of $\tilde{\Omega}_1 > \tilde{\Omega}_2 \neq 0$, the frequency cutoff of the symmetric SPP mode is equal to $\tilde{\Omega}_2$.

At first sight it seems that there are no modes at frequencies lower than $\tilde{\Omega}_2$ and therefore we have a limitation on the maximum possible operating wavelength of the QCL. Actually,

the physical background of the limitation is more complicated due to anisotropy of the waveguide core dielectric function. We return to this problem in Sec. VI.

In the case where $\tilde{\Omega}_2 \neq 0$ the surface plasmon frequency is given by the expression^{14,15,19}

$$\tilde{\Omega}_{\text{sp}} = \sqrt{\frac{\tilde{\Omega}_1^2 + \tilde{\Omega}_2^2}{2}}. \quad (16)$$

It follows from Eqs. (8) and (9) that in the general case the total number of waveguide modes N is given by the expression

$$N = \left[\frac{\sqrt{\tilde{\Omega}_1^2 - \tilde{\Omega}_2^2}}{2} \right] + \left[\frac{\sqrt{\tilde{\Omega}_1^2 - \tilde{\Omega}_2^2} + 1}{2} \right] + 3. \quad (17)$$

D. Plasma frequency of waveguide cladding layers lower than plasma frequency of waveguide core

It is quite instructive to consider the case where $\tilde{\Omega}_2 > \tilde{\Omega}_1$.²⁰ Such parameters, for example, correspond to a slab waveguide consisting of a metal film located between two semiconductor or dielectric media. The latter is called the

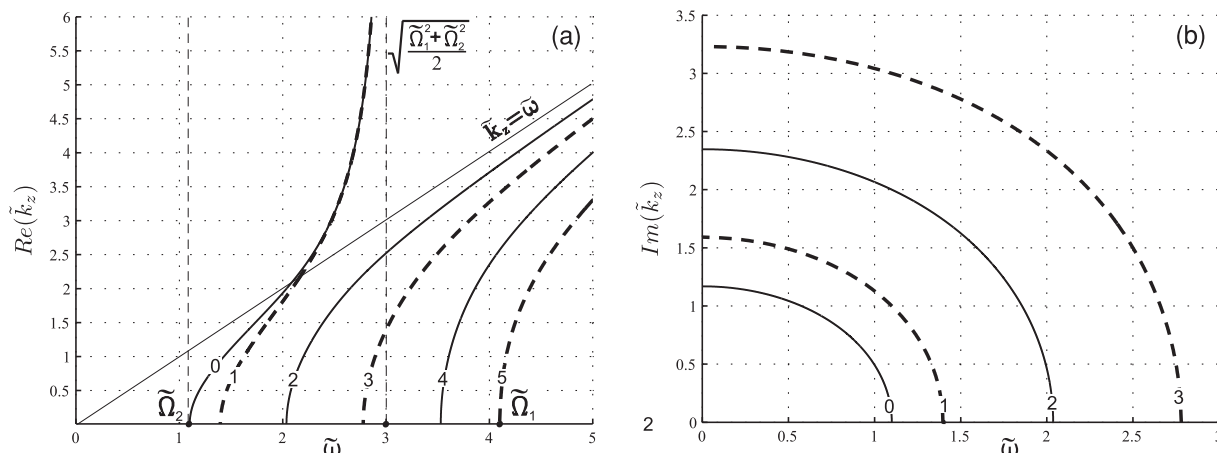


FIG. 8. (a) $\text{Re}(\tilde{k}_z)$ versus $\tilde{\omega}$; (b) $\text{Im}(\tilde{k}_z)$ versus $\tilde{\omega}$. Waveguide parameters are $\tilde{\Omega}_1 = 4.1$ and $\tilde{\Omega}_2 = 1.1$. Symmetric modes are represented by solid curves; antisymmetric modes, by dashed curves.

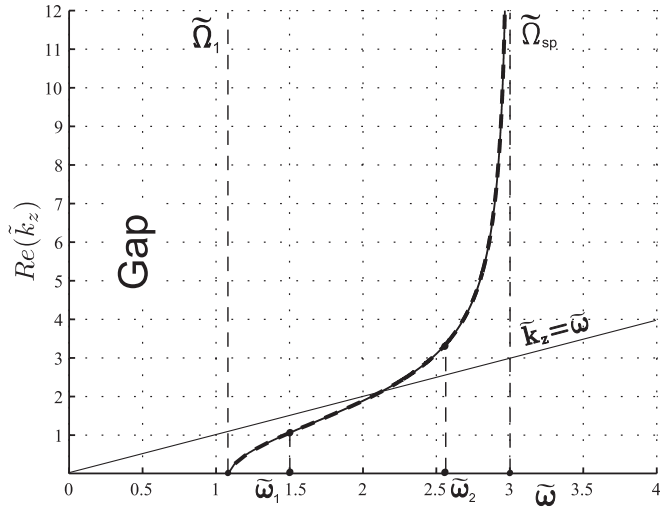


FIG. 9. $\text{Re}(\tilde{k}_z)$ versus $\tilde{\omega}$. Waveguide parameters are $\tilde{\Omega}_1 = 1.1$ and $\tilde{\Omega}_2 = 4.1$. The symmetric mode is represented by solid curves; the antisymmetric mode, by dashed curves.

insulator-metal-insulator (IMI) waveguide.⁴⁴ If $\varepsilon_1 > \varepsilon_2$, there is no total reflection from the waveguide cladding layers and there are no volume modes. However, surface modes do exist, because in the frequency range $\tilde{\Omega}_1 < \tilde{\omega} < \tilde{\Omega}_2/\sqrt{2}$ the necessary condition for SPP propagation ($\varepsilon_1 \cdot \varepsilon_2 < 0$) is fulfilled.

Let us consider a waveguide with the same parameters as in the previous section (Sec. IV C), but with the values of $\tilde{\Omega}_1$ and $\tilde{\Omega}_2$ interchanged. Therefore, $\tilde{\Omega}_1 = 1.1$ and $\tilde{\Omega}_2 = 4.1$. The dispersion characteristics of the waveguide with such parameters are shown in Fig. 9.

The dispersion curves for symmetric and antisymmetric surface modes are nearly identical. This means that the surface modes are a symmetric and antisymmetric combination of almost-nonoverlapping SPPs, as in Fig. 4. The spatial distribution of the electric field [$E_z(x)$] of the surface modes at frequencies $\tilde{\omega}_1$ and $\tilde{\omega}_2$ (see Fig. 9) is shown in Fig. 10.

The penetration depth of a single SPP in the waveguide core [$1/\text{Im}(\tilde{K})$] is maximal at $\tilde{\omega} = \tilde{\Omega}_1$ and is equal to $(\tilde{\Omega}_2^2 - \tilde{\Omega}_1^2)^{-\frac{1}{2}}$. Interference of single SPPs can be essential if the penetration depth in the waveguide core is comparable to the waveguide core thickness, that is, $\tilde{\Omega}_2^2 - \tilde{\Omega}_1^2 \sim 1$. In this case, interference

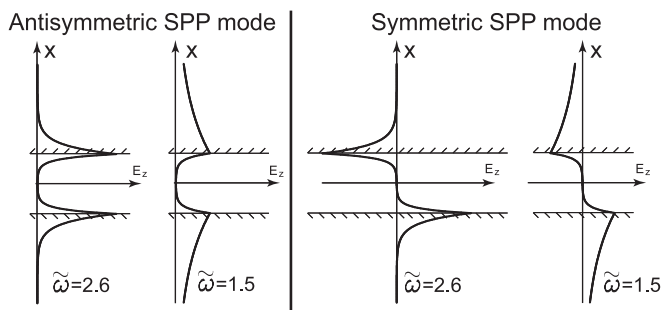


FIG. 10. Distribution of electric field z component [$E_z(x)$] for surface modes at frequencies $\tilde{\omega}_1 = 1.5$ and $\tilde{\omega}_2 = 2.6$, indicated in Fig. 9. Waveguide parameters are $\tilde{\Omega}_1 = 1.1$ and $\tilde{\Omega}_2 = 4.1$.

of SPPs results in a difference in dispersion characteristics between symmetric and antisymmetric modes [see Fig. 11(a)].

If $0 < \tilde{\Omega}_2^2 - \tilde{\Omega}_1^2 \ll 1$, then the dispersion characteristic of the symmetric surface mode $\text{Re}(\tilde{k}_z(\tilde{\omega}))$ is a multiple-valued function and the phenomenon of the negative dispersion is observed [see Fig. 11(b)]. It follows from Eq. (8) that the dispersion characteristic of symmetric surface mode is governed by the parameter θ :

$$\theta = \tilde{\Omega}_1^2 - \tilde{\Omega}_2^2. \quad (18)$$

In Fig. 12 we track the modification of the symmetric surface mode dispersion curve with the variation of θ (Fig. 12).

A numerical analysis of Eq. (8) shows that the single-valued dependence $\text{Re}(\tilde{k}_z(\tilde{\omega}))$ breaks at $-0.217 < \theta < 0$. Propagation of the symmetric surface mode at frequencies $\tilde{\omega} > \tilde{\Omega}_{\text{sp}}$ [see (16)] is possible if $-0.178 < \theta < 0$.

In the mode structure analysis of the waveguide, three parameters take part: the plasma frequencies of the cladding layers and core ($\tilde{\Omega}_1$ and $\tilde{\Omega}_2$) and the core thickness (a). If we use dimensionless quantities, we have two parameters only ($\tilde{\Omega}_1$ and $\tilde{\Omega}_2$), but all qualitatively different mode structures of the waveguide can be classified using just one parameter, θ . This parameter governs the mode number in the waveguide (10) and the peculiarities of dispersion characteristics such as negative dispersion and ambiguity of the dependence $\text{Re}(\tilde{k}_z(\tilde{\omega}))$. Classification of waveguides with qualitatively different mode structures is shown in Fig. 13.

V. NATURE OF NEGATIVE DISPERSION

In this section we consider negative dispersion in detail and explain the nature of this phenomenon. Let an SPP wave be propagating along a plane interface separating two nondissipative media with frequency-dependent dielectric functions $\varepsilon_1(\omega)$ and $\varepsilon_2(\omega)$. The latter are determined by Eq. (1). For definiteness, let $\Omega_1 > \Omega_2$. This means, for instance, that the first medium (with $s = 1$) is a metal and the second one (with $s = 2$) is a doped semiconductor. The inverse penetration depth of the SPP field is given by the expression

$$\kappa_s = \sqrt{k_z^2 - \left(\frac{\omega}{c}\right)^2 + \left(\frac{\Omega_s}{c}\right)^2}, \quad s = 1, 2. \quad (19)$$

It follows from $\Omega_1 > \Omega_2$ that $\kappa_1 > \kappa_2$. The SPP dispersion characteristic given by the expression^{14,15,19}

$$k_z(\omega) = \sqrt{\frac{\varepsilon_1(\omega)\varepsilon_2(\omega)}{\varepsilon_1(\omega) + \varepsilon_2(\omega)} \frac{\omega}{c}} \quad (20)$$

is shown in Fig. 14.

Lines of the electric field for an SPP are presented in Fig. 15(a) and the spatial distribution of the electric field components [$E_x(x)$ and $E_z(x)$] is presented in Figs. 15(b) and 15(c). The SPP magnetic field is perpendicular to the figure plane. Note that the sign of $E_x(x)$ changes in passing through the interface, that is, at $x = 0$.

The directions of the group velocity and the Poynting vector, \mathbf{S} , of an electromagnetic wave are coincident. The

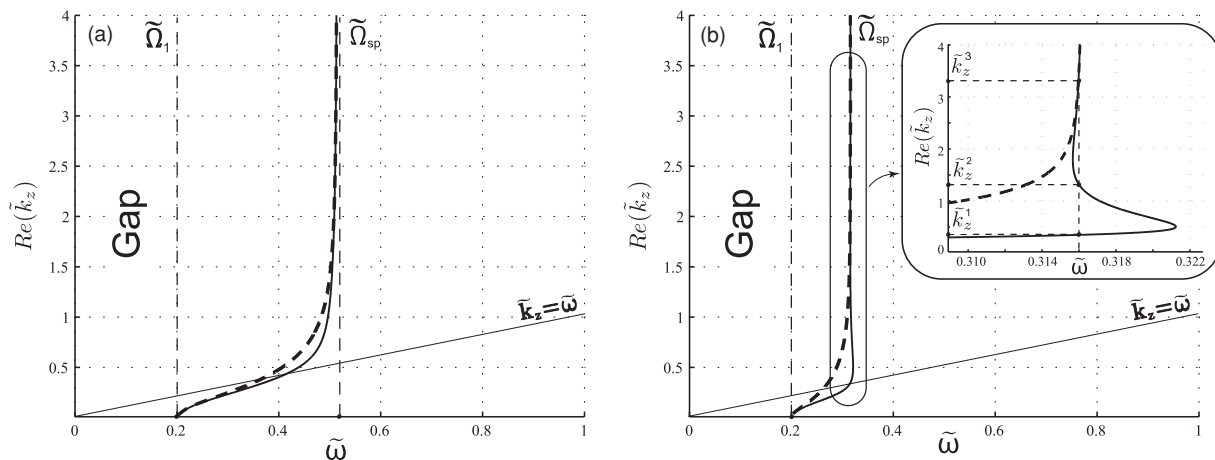


FIG. 11. (a) Dispersion characteristics of surface modes at $\tilde{\Omega}_2^2 - \tilde{\Omega}_1^2 \sim 1$. Waveguide parameters are $\tilde{\Omega}_1 = 0.2$, $\tilde{\Omega}_2 = 0.7$. (b) Dispersion characteristics of surface modes at $\tilde{\Omega}_2^2 - \tilde{\Omega}_1^2 \ll 1$. Waveguide parameters are $\tilde{\Omega}_1 = 0.2$, $\tilde{\Omega}_2 = 0.4$. The symmetric mode is represented by the solid curve; the antisymmetric mode, by the dashed curve.

Z component of the Pointing vector in an arbitrary point of the waveguide is given by the expression⁸

$$S_z = \frac{c}{8\pi} \text{Re}\{[\mathbf{E}\mathbf{H}^*]_z\}. \quad (21)$$

It can be simplified using Eq. (6):

$$S_{sz} = \frac{\omega}{8\pi} \text{Re} \left\{ \frac{\epsilon_s}{k_z} \right\} |E_{sx}|^2, \quad s = 1, 2. \quad (22)$$

It follows from (22) that inside the metal ($s = 1$) the directions of S_{1z} and k_z are opposite, $\epsilon_1(\omega) < 0$, and inside the semiconductor ($s = 2$) the directions of S_{2z} and k_z are the

same, $\epsilon_2(\omega) > 0$. The total energy flux I of the SPP per the unity of width is

$$I = \int_{-\infty}^0 S_{2z} dx + \int_0^{\infty} S_{1z} dx. \quad (23)$$

As the SPP penetration depth inside the metal ($s = 1$) is less than that inside the semiconductor ($s = 2$), the direction of total energy flux of the SPP, I , coincides with the direction of k_z . As a result, the directions of the group and phase velocities of the SPP are coincident. Therefore, there is no negative dispersion.

At ω close to Ω_{sp} , the penetration depths inside both media are the same ($\kappa_1 \approx \kappa_2$) and the dielectric functions are opposite

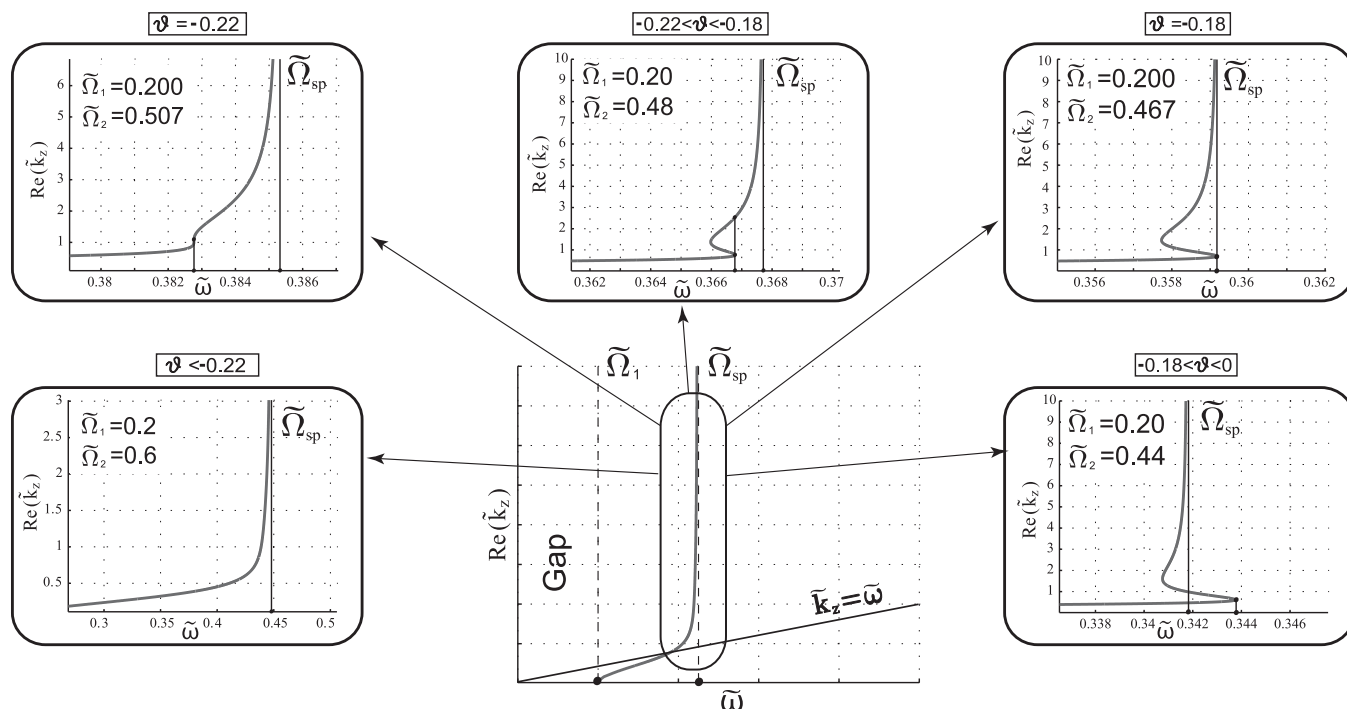


FIG. 12. Dependence of $\text{Re}(\tilde{k}_z(\tilde{\omega}))$ for a symmetric surface mode at different θ values.

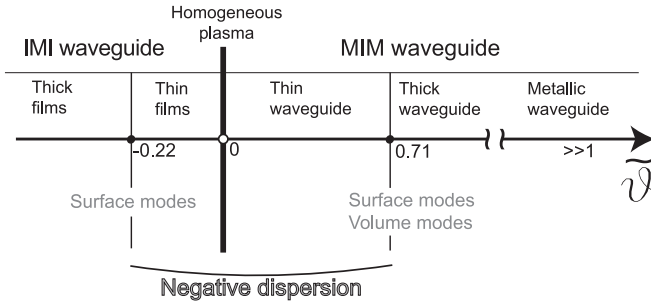


FIG. 13. Classification of the possible mode structures in a three-layered slab waveguide. The type of mode structure is determined by the parameter θ .

($\varepsilon_1 \approx -\varepsilon_2$). Therefore, according to Eqs. (22) and (23), $I \rightarrow 0$ as $\omega \rightarrow \Omega_{sp}$; that is, the group velocity of SPP tends to 0 (see Fig. 14).

In a planar metal-insulator-metal (MIM) waveguide, a symmetric SPP mode forms due to the constructive interference of surface waves and an antisymmetric SPP mode forms due to the destructive interference of surface waves. Under destructive interference, x components of the electric field, E_x , are subtracted. Therefore, according to (22), the energy flux decreases inside the waveguide core. If the overlapping of E_x is pronounced, the energy flux inside the waveguide core can be less than the energy flux inside the cladding layers. Therefore, the direction of the total energy flux and the group velocity are opposite to the phase velocity, that is, to the direction of k_z . Thus, there is a negative dispersion. For the symmetric surface mode, interference is constructive and x components of the electric field, E_x , are summarized. As a result, dispersion for the symmetric SPP mode is positive.

Similar reasoning in the case of an IMI waveguide shows that the negative dispersion phenomenon can be observed in a thin waveguide only for the symmetric SPP mode. Dispersion for the antisymmetric SPP mode is always positive in this case.

The phenomenon of negative dispersion can be observed for the volume modes if the penetration depth inside the cladding layers is large. This condition can be fulfilled for volume modes with a frequency cutoff close to the plasma frequency of the waveguide cladding layers (see Fig. 16).

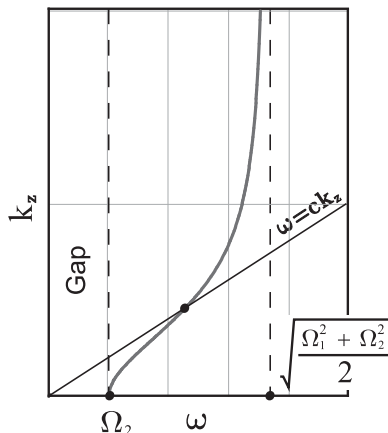


FIG. 14. SPP dispersion characteristic; $\Omega_1 > \Omega_2$.

VI. MODE STRUCTURE OF A WAVEGUIDE WITH AN ANISOTROPIC CORE

A. Dielectric function of the waveguide core

Until now, we have ignored active and injector sections and considered dielectric function of the waveguide core as a scalar. In this section we analyze the mode structure of the waveguide under the assumption that a considerable part of the core is occupied by the alternate active and injector sections.⁴ In this case, we should regard the dielectric function of the waveguide core as a tensor, (3).

In this section, we neglect FCA and amplification. Thus, components of the dielectric function (ε_{\parallel} and ε_{\perp}) are real. We take into account imaginary parts of the dielectric functions in Sec. VII. For a layered structure within approximation of the continuum medium, the longitudinal and transversal tensor components of the dielectric functions ε_{\parallel} and ε_{\perp} are⁴⁵

$$\varepsilon_{\parallel} = \xi \varepsilon_{\parallel}^a + (1 - \xi) \varepsilon_{\parallel}^i, \quad (24)$$

$$\frac{1}{\varepsilon_{\perp}} = \frac{\xi}{\varepsilon_{\perp}^a} + \frac{1 - \xi}{\varepsilon_{\perp}^i}. \quad (25)$$

Here, $\varepsilon_{\perp, \parallel}^{i, a}$ are the transversal and longitudinal components of the injector and active regions, and ξ is a thickness fraction of the core occupied by active sections. Equation (24) is justified in the case of slow spatial variations of the longitudinal electric field component on the SL period, d . Equation (25) is justified if the same condition is fulfilled for the electric displacement field.⁴⁵

Injector sections are SLs. Electron states inside them form energy minibands.⁴ Therefore, one can regard electron motion normal to the SL layers as free. This statement is correct regarding electron motion along the SL layers. It allows us to describe the longitudinal and transversal components of the injector dielectric function ($\varepsilon_{\parallel}^i, \varepsilon_{\perp}^i$) within the Drude-Lorentz approximation (1), using longitudinal and transversal plasma frequencies: $\tilde{\Omega}_{\perp}^i$ and $\tilde{\Omega}_{\parallel}^i$. For an injector region $\tilde{\Omega}_{\perp}^i < \tilde{\Omega}_{\parallel}^i$, because the low-energy effective mass of an electron moving perpendicular to the SL layers is expected to be greater than that of an electron moving along the SL layers ($m_{\perp}^{i*} > m_{\parallel}^{i*}$). The longitudinal component of the dielectric function in the active region $\varepsilon_{\parallel}^a$ is described according to the Drude-Lorentz approximation (1) using the longitudinal plasma frequency $\tilde{\Omega}_{\parallel}^a$, because electron motion is free along the layers of the active region.

Neglect of amplification and losses implies that we disregard tunnel current through active sections. Therefore, electrons can move only along the active-region layers. So we can set $m_{\perp}^{a*} = \infty$ and $\tilde{\Omega}_{\perp}^a = 0$ and consider ε_{\perp}^a as a constant within the first approximation:

$$\varepsilon_{\perp}^a(\omega) = \varepsilon^{\infty}. \quad (26)$$

First, we consider two opposite cases.

(1) The thickness of the injector section is much less than the thickness of the active section. This means that we can set $\xi = 1$ in (24) and (25).

(2) The thickness of the active section is much less than that of the injector section. This means that we can set $\xi = 0$ in (24) and (25).

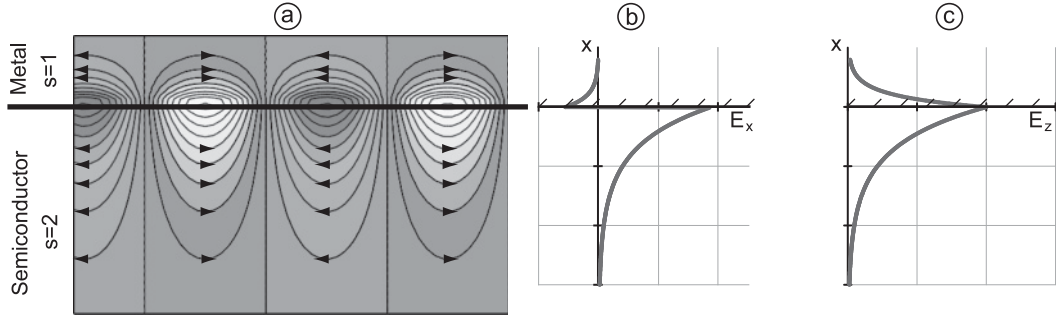


FIG. 15. (a) Lines of the SPP electric field [$E_x(x)$ and $E_z(x)$]. (b) Distribution of the electric field x component [$E_x(x)$]. (c) Distribution of the electric field z component [$E_z(x)$].

B. Waveguide core free of injector sections

Here, we consider the mode structure of a waveguide free of injector sections ($\xi = 1$). It follows from (24) and (25) that the longitudinal and transversal components of the waveguide core dielectric function are

$$\varepsilon_{\parallel} = \varepsilon^{\infty} \left(1 - \frac{\tilde{\Omega}_{\parallel}^2}{\tilde{\omega}^2} \right), \quad \varepsilon_{\perp} = \varepsilon^{\infty}. \quad (27)$$

Let the dimensionless waveguide parameters be $\tilde{\Omega}_1 = 4.1$, $\tilde{\Omega}_{\perp}^a = 0$, and $\tilde{\Omega}_{\parallel}^a = 1.1$. For example, such parameters correspond to a waveguide with an $a = 8 \mu\text{m}$ active region core sandwiched between n -doped GaAs ($n_{1,3} = 5 \times 10^{18} \text{ 1/cm}^3$) cladding layers. The electron concentration in the waveguide core is $n_2 = 3.5 \times 10^{17} \text{ 1/cm}^3$. For simplicity, we regard the longitudinal effective electron mass in the core and in the cladding layers to be the same.

The mode structure of a waveguide with an anisotropic core is shown in Fig. 17(a). In comparison with the case of an isotropic core (see Sec. IV), there are additional electromagnetic modes. They are shown by the dashed ellipses in Fig. 17(a). The number of these modes is infinite, but in Fig. 17(a) we show only four of them. The wave vector \tilde{k}_z for

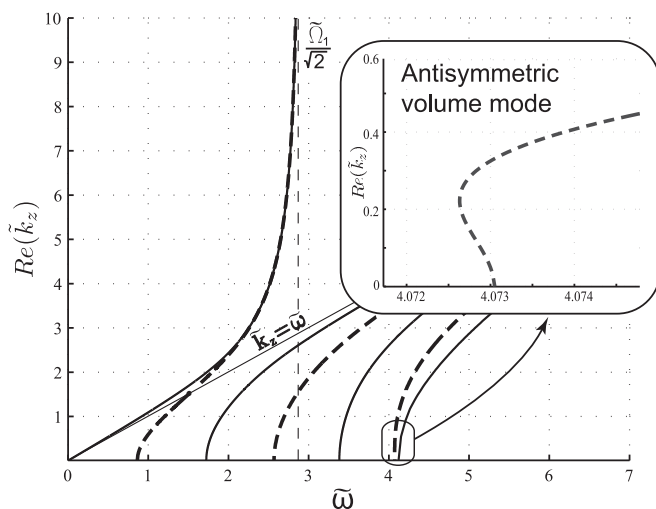


FIG. 16. $\text{Re}(\tilde{k}_z)$ versus $\tilde{\omega}$. Waveguide parameters are $\tilde{\Omega}_1 = 4.1$ and $\tilde{\Omega}_2 = 0$. Symmetric modes are represented by solid curves; antisymmetric modes, by dashed curves.

all of these modes tends to infinity as $\tilde{\omega} \rightarrow \tilde{\Omega}_{\parallel}^a$. There are no frequency cutoffs for them or for the symmetric surface mode.

The distribution of the electric field [$E_z(x)$] for these modes is shown in Fig. 18. The indexes for the modes with singularity coincide with the number of humps of the function $E_z(x)$.

The statement that the number of modes with singularity at $\tilde{\Omega}_{\parallel}^a$ is infinite is correct only within the continuum medium approximation. This approximation is not justified for modes with singularity at $\tilde{\Omega}_{\parallel}^a$ if their indexes are more than the number of SL periods. Therefore, the quantity of these modes is finite and is approximately equal to the number of SL periods.

In contrast to the case of a waveguide with an isotropic core, \tilde{k}_z can be not equal to zero at the frequency cutoff for a volume mode [Figs. 17(a) and 17(b)]. A similar situation takes place in dielectric waveguides.³

C. Thick injector sections

In this section we consider another extreme case, where the whole space between cladding layers is filled up only by injector sections ($\xi = 0$). Then it follows from (24) and (25) that the longitudinal and transversal components of the waveguide core dielectric function are

$$\varepsilon_{\parallel} = \varepsilon^{\infty} \left(1 - \frac{\tilde{\Omega}_{\parallel}^2}{\tilde{\omega}^2} \right), \quad \varepsilon_{\perp} = \varepsilon^{\infty} \left(1 - \frac{\tilde{\Omega}_{\perp}^2}{\tilde{\omega}^2} \right). \quad (28)$$

The mode structure shown in Fig. 17(b) is calculated for a waveguide with the following dimensionless parameters: $\tilde{\Omega}_{\parallel}^i = 1.1$, $\tilde{\Omega}_{\perp}^i = 0.4$, and $\tilde{\Omega}_1 = 4.1$. They correspond, for example, to a waveguide with n -doped GaAs ($n_{1,3} = 5 \times 10^{18} \text{ 1/cm}^3$) cladding layers, with an $8\text{-}\mu\text{m}$ n -doped ($n_2 = 3.5 \times 10^{17} \text{ 1/cm}^3$) waveguide core. We set the longitudinal and transversal effective masses of an electron in the waveguide core at $m_{\parallel}^{i*} = 0.07m_e$ and $m_{\perp}^{i*} = 0.5m_e$.

In this case the symmetric surface mode and modes with singularity at $\tilde{\omega} = \tilde{\Omega}_{\parallel}^i$ have a common frequency cutoff equal to $\tilde{\Omega}_{\perp}^i$ [Fig. 17(b)]. Therefore, modes with singularity at $\tilde{\omega} = \tilde{\Omega}_{\parallel}^i$ exist in the frequency range $\tilde{\Omega}_{\perp}^i < \tilde{\omega} < \tilde{\Omega}_{\parallel}^i$. Hence, in our approximation, the maximum operation wavelength of the QCL is controlled by the electron concentration of the injector layers.

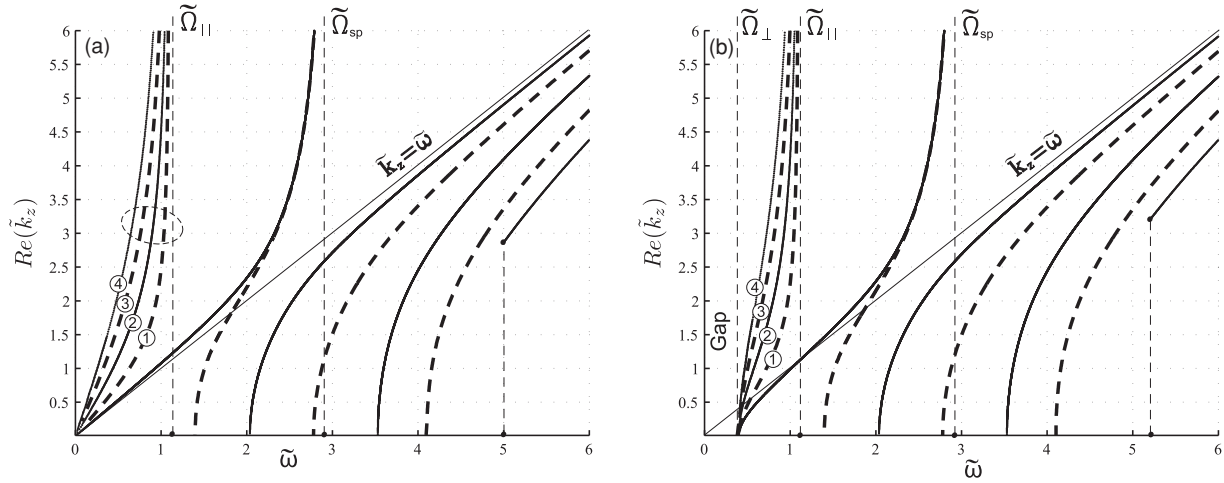


FIG. 17. $\text{Re}(\tilde{k}_z)$ versus $\tilde{\omega}$ for a waveguide with an anisotropic core. (a) Waveguide parameters are $\xi = 1$, $\tilde{\Omega}_{\parallel}^a = 1.1$, $\tilde{\Omega}_{\perp}^a = 0$, and $\tilde{\Omega}_1 = 4.1$. (b) Waveguide parameters are $\xi = 0$, $\tilde{\Omega}_{\parallel}^i = 1.1$, $\tilde{\Omega}_{\perp}^i = 0.4$, and $\tilde{\Omega}_1 = 4.1$. Symmetric modes are represented by solid curves; antisymmetric modes, by dashed curves.

The frequency of a surface plasmon $\tilde{\Omega}_{\text{sp}}$, in this case is

$$\tilde{\Omega}_{\text{sp}} = \sqrt{\frac{\tilde{\Omega}_1^4 - \tilde{\Omega}_{\parallel}^2 \tilde{\Omega}_{\perp}^2}{2\tilde{\Omega}_1^2 - \tilde{\Omega}_{\parallel}^2 - \tilde{\Omega}_{\perp}^2}}. \quad (29)$$

Langmuir modes are nearly transversal ($|E_z| \ll |E_x|$) at $\tilde{\omega} = \tilde{\Omega}_{\perp}^i$ and nearly longitudinal ($|E_x| \ll |E_z|$) at $\tilde{\omega} = \tilde{\Omega}_{\parallel}^i$. Therefore, the electric field of these modes induces polarization of waveguide materials only in the x direction at $\tilde{\omega}$ close to $\tilde{\Omega}_{\perp}^i$ and in the z direction at $\tilde{\omega}$ close to $\tilde{\Omega}_{\parallel}^i$.

The nature of these modes is as follows. In plasma, there are Langmuir waves.⁴⁶ These are longitudinal waves with a frequency usually almost independent of wave number. In this case, infinite degeneracy takes place: infinitely many wave numbers correspond to the same value of the plasma frequency. In anisotropic plasma, when the frequency of plasma oscillation depends on the direction, the degeneracy is partly lifted. Thus, the frequency of the wave depends on the direction of the wave vector, and not on its absolute value. If we interpose the plasma between two parallel perfectly conducting surfaces, the Langmuir wave reflects from the surfaces. Thus, the component of the wave vector normal to the surfaces, K , is proportional to the arbitrary integer number. Each dispersion curve with singularity at $\tilde{\Omega}_{\parallel}^i$ [see Fig. 17(b)] corresponds to a certain fixed value of K . Therefore, it is natural enough to call these modes Langmuir modes.

Langmuir modes exist in a waveguide with an isotropic core. This fact can be made clear by means of a passage to

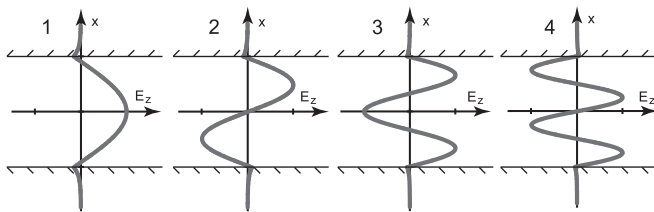


FIG. 18. Distribution of the electric field z component [$E_z(x)$] for the modes labeled 1–4 in Fig. 17(a). Here $\tilde{\omega} = 0.5$.

the limit $\tilde{\Omega}_{\parallel} \rightarrow \tilde{\Omega}_{\perp}$, keeping $\tilde{\omega}$ between $\tilde{\Omega}_{\parallel}$ and $\tilde{\Omega}_{\perp}$. The frequency of Langmuir modes is equal to the plasma frequency of the core and does not depend on the wave number. So as not to overload the figures, we do not plot dispersion curves of Langmuir modes in the case of an isotropic waveguide core.

D. Arbitrary thickness of injector and active sections

It follows from (24) and (25) that in the case of arbitrary thickness of the injector and active sections, the longitudinal and transversal components of the waveguide core dielectric function are

$$\varepsilon_{\parallel} = \varepsilon^{\infty} \left(1 - \frac{\tilde{\Omega}_{\parallel}^2}{\tilde{\omega}^2} \right), \quad (30)$$

$$\varepsilon_{\perp} = \varepsilon^{\infty} \frac{\tilde{\omega}^2 - \tilde{\Omega}_{\perp}^2}{\tilde{\omega}^2 - \xi \tilde{\Omega}_{\perp}^2}, \quad (31)$$

where $\tilde{\Omega}_{\parallel}^2 = \xi \tilde{\Omega}_{\parallel}^a + (1 - \xi) \tilde{\Omega}_{\parallel}^i$. Frequency dependence of the dielectric function (31) is peculiar to ionic crystals.⁴⁷

The pole in the denominator of Eq. (31) states that electron motion perpendicular to the waveguide core layers is not free. It is due to the active sections, which separate injector sections and restrict electrons inside them. In macroscopic approximation, this is equivalent to a restoring force that acts on electrons along the SL axis. The pole corresponds to the eigenfrequency of the oscillation due to the restoring force.

Usually, the thicknesses of injector and active sections have a similar order of magnitude.⁴ So let us consider the mode structure of a waveguide with the following dimensionless parameters: $\xi = 0.5$, $\tilde{\Omega}_1 = 4.1$, $\tilde{\Omega}_{\parallel}^i = 1.7$, $\tilde{\Omega}_{\perp}^i = 0.4$, and $\tilde{\Omega}_{\parallel}^a = 0.5$. They correspond, for example, to a waveguide with n -doped GaAs ($n_{1,3} = 5 \times 10^{18} \text{ 1/cm}^3$) cladding layers, with an 8- μm waveguide core. The electron concentration is $8 \times 10^{17} \text{ 1/cm}^3$ inside injector sections and $7 \times 10^{16} \text{ 1/cm}^3$ inside active sections. The longitudinal effective mass of an electron in the injector and active sections is $m_{\parallel}^{i*} = 0.07m_e$.

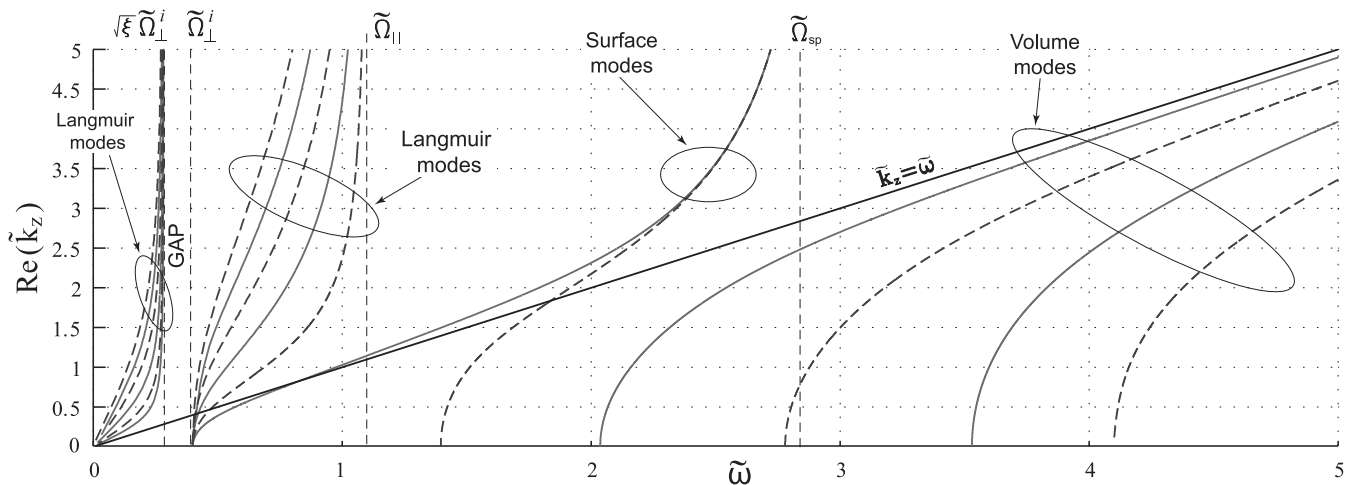


FIG. 19. Waveguide parameters are $\xi = 0.5$, $\tilde{\Omega}_\perp = 4.1$, $\tilde{\Omega}_\parallel^i = 1.1$, $\tilde{\Omega}_\perp^i = 0.4$, and $\tilde{\Omega}_\parallel^a = 1.1$. Symmetric modes are represented by solid curves; antisymmetric modes, by dashed curves.

The transversal effective mass of an electron in injector sections is $m_\perp^{i*} = m_e$.

The mode structure of a waveguide with such parameters is shown in Fig. 19. In contrast to the case of a resonator free of injector sections (see Sec. VIB), there is a frequency gap for Langmuir modes. At the lower edge of the gap, $\sqrt{\xi}\tilde{\Omega}_\perp^i$, the z component of the wave vector, \tilde{k}_z , tends to infinity and the wave becomes nearly longitudinal. At the upper bound of the gap, $\tilde{\Omega}_\perp^i$, the z component of the wavevector is equal to 0 ($\tilde{k}_z = 0$) and the wave is transversal.

The nature of the gap for Langmuir modes is as follows. At the frequency $\sqrt{\xi}\tilde{\Omega}_\perp^i$ there is a resonance due to the effective restoring force. Above the resonance frequency we can roughly consider electrons to be free in the direction normal to the SL layers. Free electrons in the waveguide core result in a frequency gap below the plasma frequency (see Sec. VIC). Therefore, at the frequencies $\sqrt{\xi}\tilde{\Omega}_\perp^i < \tilde{\omega} < \tilde{\Omega}_\perp^i$ there is a gap.

The analytical solution for the dependence $\tilde{k}_z(\tilde{\omega})$ can be found in the case of perfectly conducting waveguide cladding layers ($\tilde{\Omega}_1 \gg 1$) for an arbitrary value of ξ . In this case, we regard the electromagnetic wave as being confined strictly inside the waveguide core. The analytical solution of Eqs. (8) and (9) is

$$\tilde{k}_z = \sqrt{\varepsilon_\perp \left(\tilde{\omega}^2 - \frac{n^2}{\varepsilon_\parallel} \right)}. \quad (32)$$

Here, n is the index of the mode, that is, any integer number equal to the quantity of the humps.

In this case, amplitude ratio of the transversal electric field component to the longitudinal one is defined as

$$\frac{E_x}{E_z} = -\frac{\tilde{k}_z \varepsilon_\parallel}{\tilde{K} \varepsilon_\perp}. \quad (33)$$

VII. FREE CARRIER ABSORPTION ANALYSIS

Until now, we have neglected the energy dissipation and analyzed mode structure only. In this section we analyze

optical losses. Experimental data and numerical modeling confirm that the main mechanisms of the optical losses in QCLs are FCA and intersubband absorption.^{48–50} An analysis of intersubband absorption is presented in Refs. 50 and 51. Here, we analyze the spectrum of optical losses only due to FCA. We take FCA into account within the Drude-Lorentz approximation, (1).

In the general case, the dielectric function of the waveguide core is a tensor, (3). FCA absorption is apparently anisotropic in the waveguide core. It is possible to divide FCA into transversal (due to E_x) and longitudinal (due to E_z) FCA. Each of them can be estimated within the Drude-Lorentz approximation by means of longitudinal and transversal inverse momentum relaxation times, γ_\parallel and γ_\perp [see Eq. (1)]. However, in this paper we restrict our analysis of FCA to the case of a waveguide with an isotropic core.

The attenuation coefficient $\tilde{\alpha}_w$ is defined as follows:

$$\tilde{\alpha}_w = 2\text{Im}(\tilde{k}_z). \quad (34)$$

Further, we analyze the frequency dependence of $\text{Im}(\tilde{k}_z)$.

The wave attenuation is caused by two factors. The first is that there is no propagating wave in the spectral gap. The second factor is real absorption. In contrast to the wave attenuation due to the spectral gap, real absorption tends to 0 along with the inverse momentum relaxation time, γ .

A. Semiconductor cladding layers

Here we consider a GaAs waveguide with an 8- μm thickness n -doped core ($n_2 = 1 \times 10^{16} \text{ 1/cm}^3$) and n -doped cladding layers ($n_{1,3} = 5 \times 10^{18} \text{ 1/cm}^3$). In terms of dimensionless quantities, the waveguide parameters are $\tilde{\Omega}_1 = 4.1$ and $\tilde{\Omega}_2 = 0.18$.

Supposing a momentum relaxation time equal to 0.1 ps for cladding layers and to 0.5 ps for waveguide core we have the dimensionless parameters $\tilde{\gamma}_1 = 0.29$ and $\tilde{\gamma}_2 = 0.06$.

The frequency dependence of the imaginary part of \tilde{k}_z is shown in Fig. 20(a). To distinguish the attenuation coefficients due to FCA and due to the spectral gap, we show the boundary

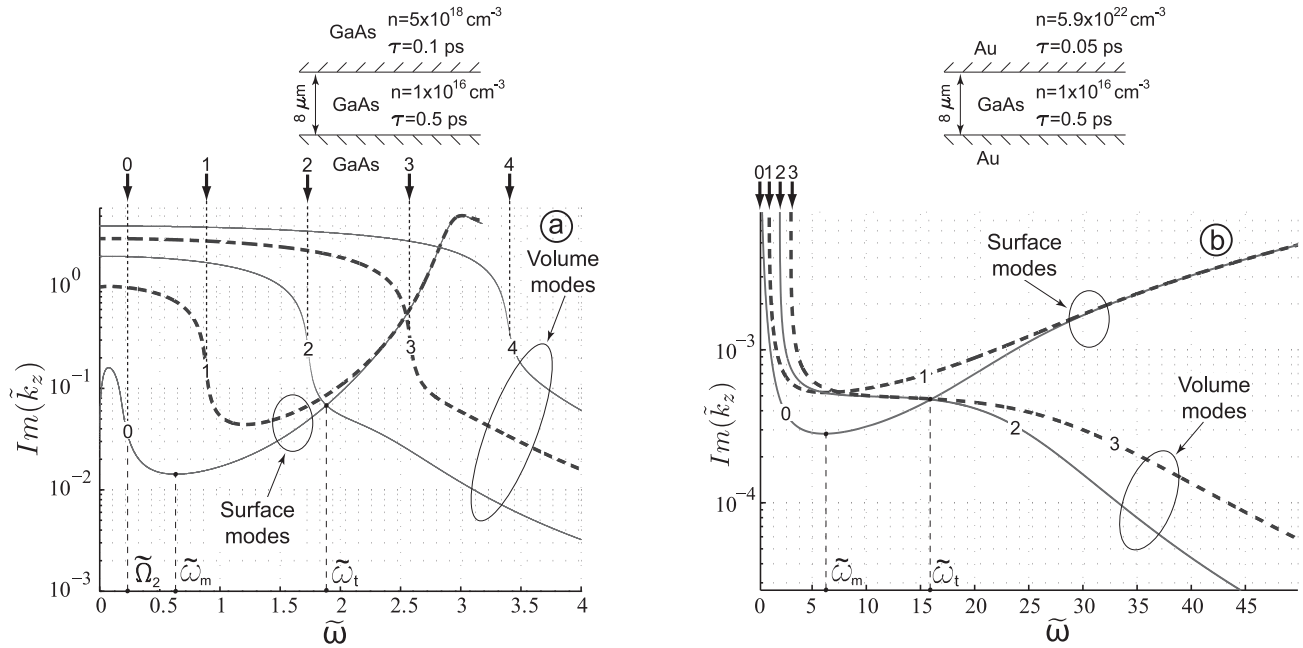


FIG. 20. (a) $\text{Im}(\tilde{k}_z)$ versus $\tilde{\omega}$; waveguide parameters are $\tilde{\Omega}_1 = 4.1$, $\tilde{\Omega}_2 = 0.18$, $\tilde{\gamma}_1 = 0.29$, and $\tilde{\gamma}_2 = 0.06$. (b) $\text{Im}(\tilde{k}_z)$ versus $\tilde{\omega}$. Waveguide parameters are $\tilde{\Omega}_1 = 396$, $\tilde{\Omega}_2 = 0.18$, $\tilde{\gamma}_1 = 0.58$, and $\tilde{\gamma}_2 = 0.06$. Symmetric modes are represented by solid curves; antisymmetric modes, by dashed curves.

of the spectral gap by numbered arrows [see Fig. 20(a)]. The numbers of the arrows correspond to the indexes of the modes.

FCA is minimal for the symmetric surface mode at low frequencies. FCA for this mode increases with frequency, in contrast to FCA for volume modes. FCA for the first symmetric volume mode is equal to FCA for the symmetric surface mode at frequency $\tilde{\omega}_t$ [see Fig. 20(b)]. At frequencies higher than $\tilde{\omega}_t$, FCA is minimal for the first symmetric volume mode. FCA decreases with frequency roughly as $\tilde{\omega}^2$ (see, e.g., Ref. 3). The frequency $\tilde{\omega}_t$ corresponds to the wavelength $29 \mu\text{m}$. For the symmetric surface mode, FCA has a minimum between the frequency cutoff, $\tilde{\Omega}_2$, and the frequency of the surface plasmon, $\tilde{\Omega}_{\text{sp}}$. The minimum is reached at the frequency $\tilde{\omega}_m$, which corresponds to the wavelength $86 \mu\text{m}$.

At a fixed frequency, the higher the frequency cutoff of the volume mode, the greater the FCA for it [see Figs. 20(a) and 20(b)]. In Sec. IV A we noted that this occurs because the penetration depth of the volume modes inside the cladding layers increases with the frequency cutoff (see Fig. 5).

The minimal attenuation coefficient for the symmetric surface mode is equal to 112 cm^{-1} (at $86 \mu\text{m}$). These are very high losses. Usually intersubband absorption in QCL is approximately or less than 20 cm^{-1} (e.g., see Refs. 51 and 50). Therefore, using the symmetric surface mode in a QCL with semiconductor claddings is not favorable. It is more reasonable to use a waveguide with metal cladding layers.^{10,11}

B. Metal cladding layers

In Fig. 20(b), we show the attenuation coefficient for a waveguide with cladding layers made of gold. Other parameters are the same as in the previous example [see Fig. 20(a)]. Dimensionless parameters for the gold cladding

layers are $\tilde{\Omega}_1 = 396$ and $\tilde{\gamma}_1 = 0.58$. They correspond to a plasma frequency of $\tilde{\Omega}_1 = 2.18 \times 10^{15} \text{ s}^{-1}$ and a momentum relaxation time of 0.05 ps . In Fig. 20(b) we show only two surface modes and two volume modes. The total number of modes in such a waveguide is $\sim \tilde{\Omega}_1$ (10).

In the waveguide with gold cladding layers the attenuation coefficient for the symmetric surface mode is equal to 22 cm^{-1} (at $86 \mu\text{m}$). The minimal attenuation coefficient for the symmetric surface mode is equal to 2.2 cm^{-1} . The minimum loss for the symmetric surface mode is reached at $8.9 \mu\text{m}$.

In the case of an isotropic waveguide core the maximum operating wavelength is limited by the plasma frequency of the core, $\tilde{\Omega}_2$ [Figs. 20(a) and 20(b)], that is, by concentration of free carriers in the core. In the case of an anisotropic waveguide core there is no limitation on the maximum operating wavelength, because Langmuir modes can be excited at an arbitrarily low frequency (see Fig. 19).

Analysis of FCA in a waveguide with an anisotropic core can be done easily in the case of perfectly conducting cladding layers. In this case, the frequency dependence of \tilde{k}_z is determined by Eq. (32). Therefore, to get the frequency dependence of $\text{Im}(\tilde{k}_z)$, it is necessary to substitute the complex dielectric function, (24) and (25), in (32). This consideration is beyond the scope of this paper.

VIII. CONCLUSION

In this paper, we have presented a detailed analysis of the mode structure of a QCL cavity, taking into account the surface and volume modes jointly. Even within the simple model of a QCL cavity, the mode structure is quite complicated. Nevertheless, it is possible to classify all the varieties of mode structures using one dimensionless parameter, θ [Eq. (18)].

We have shown that the frequency dependencies of FCA are opposite for the surface and volume modes: FCA for surface modes increases with frequency, while that for volume modes decreases.

In the THz region the symmetric SPP mode has several advantages over other modes. In the THz region, the symmetric SPP mode is nearly transversal. Therefore, the electric field does not induce losses due to longitudinal electron motion in SL layers and stimulates mainly laser transitions. In the case of an isotropic waveguide core, the frequency cutoff for the symmetric SPP mode is determined only by the free electron concentration in the waveguide core and does not depend on the waveguide core thickness. Being almost totally localized within waveguide core at the THz frequencies, the symmetric SPP mode has the lowest FCA.

The minimal FCA in the waveguide with metal cladding layers for the surface symmetric mode is $\sim 1 \text{ cm}^{-1}$. In this case, the main contribution to the optical losses is made by intersubband absorption, which is usually $\lesssim 20 \text{ cm}^{-1}$ (e.g., see Refs. 51 and 50). In the waveguide with semiconductor cladding layers, the main contribution to the optical losses is made by FCA. In this case, for the symmetric surface mode, minimal optical losses are $\sim 100 \text{ cm}^{-1}$.

We have shown that due to the free electrons in the waveguide core, there are Langmuir modes. We have explained the nature of these modes. The frequency of Langmuir modes does not depend on the wave number in the case of an isotropic

waveguide core. Therefore, there is a degeneracy. Anisotropy of the waveguide core lifts the degeneracy. In the case of arbitrary thicknesses of active and injector sections, there is no frequency cutoff for Langmuir modes. Therefore, these modes can be excited at arbitrary low frequencies.

We have shown that the group and phase velocities of surface and volume modes can have opposite signs; that is, there is negative dispersion phenomenon. We have explained the nature of this phenomenon and found the waveguide threshold parameter at which it appears. It follows from continuity of the dependence $\tilde{k}_z(\tilde{\omega})$ that if some mode has negative dispersion, then the group velocity of this mode is 0 at some frequency. Using the modes with a low group velocity, it is possible to obtain a high amplification coefficient of the laser and decrease the threshold current density. The same idea is used in distribution feedback lasers.^{52–54}

ACKNOWLEDGMENTS

This work was supported by the Saint Petersburg Government, by RFBR (Grant No. 08-02-01337-a), by the Program “Basic Research in Nanotechnology and Nanomaterials” of the Russian Academy of Sciences, and by the Ministry of Education and Science of the Russian Federation (Grant No. 2.1.1/988). One of the authors (A. Bogdanov) appreciates the valuable support of the Dynasty Foundation (Program for Graduate Students and Young Pre-Degree Scientists).

*bogdanftf@mail.ru

†suris@theory.ioffe.ru

¹R. Kazarinov and R. Suris, *Sov. Phys. Semicond.* **5**, 797 (1971).

²J. Faist, F. Capasso, D. Sivco, C. Sirtori, A. Hutchinson, and A. Cho, *Science* **264**, 553 (1994).

³D. Marcuse, *Theory of Dielectric Optical Waveguides* (Academic Press, New York, 1974).

⁴C. Gmachl, F. Capasso, D. Sivco, and A. Cho, *Rep. Prog. Phys.* **64**, 1533 (2001).

⁵R. Suris, in *Proceedings of the NATO Advanced Research Workshop on Future Trends in Microelectronics: Reflection on the Road to Nanotechnology, NATO ASI Series, Ser. E*, Vol. 323, edited by S. Luryi, J. Xu, and A. Zaslavsky (Kluwer Academic, New York, 1996), p. 197.

⁶N. Wingreen and C. Stafford, *IEEE J. Quantum Electron.* **33**, 1170 (1997).

⁷I. Dmitriev and R. Suris, *Phys. Status Solidi* **202**, 987 (2005).

⁸L. Landau, L. Pitaevskii, and E. Lifshitz, *Electrodynamics of Continuous Media*, 2nd ed., *Course of Theoretical Physics*, Vol. 8 (Pergamon Press, Oxford, 1984).

⁹R. Colombelli, F. Capasso, C. Gmachl, A. L. Hutchinson, D. L. Sivco, A. Tredicucci, M. C. Wanke, A. M. Sergent, and A. Y. Cho, *Appl. Phys. Lett.* **78**, 2620 (2001).

¹⁰K. Unterrainer, R. Colombelli, C. Gmachl, F. Capasso, H. Y. Hwang, A. M. Sergent, D. L. Sivco, and A. Y. Cho, *Appl. Phys. Lett.* **80**, 3060 (2002).

¹¹B. Williams, S. Kumar, H. Callebaut, Q. Hu, and J. Reno, *J. Appl. Phys.* **83**, 2124 (2003).

¹²R. Kohler, A. Tredicucci, F. Beltram, H. Beere, E. Linfield, A. Davies, D. Ritchie, R. Iotti, and F. Rossi, *Nature* **417**, 156 (2002).

¹³M. Belkin, F. Capasso, F. Xie, A. Belyanin, M. Fischer, A. Wittmann, and J. Faist, *Appl. Phys. Lett.* **92**, 201101 (2008).

¹⁴V. Agranovich and D. Mills, *Surface Polaritons* (North-Holland, Amsterdam, 1982).

¹⁵S. Maier, *Plasmonics: Fundamentals and Applications* (Springer, New York, 2007).

¹⁶R. Ritchie, *Phys. Rev.* **106**, 874 (1957).

¹⁷R. Ferrell, *Phys. Rev.* **111**, 1214 (1958).

¹⁸R. Pettit, J. Silcox, and R. Vincent, *Phys. Rev. B* **11**, 3116 (1975).

¹⁹J. Pitarke, V. Silkin, E. Chulkov, and P. Echenique, *Rep. Prog. Phys.* **106**, 1 (2007).

²⁰E. Economou, *Phys. Rev.* **182**, 539 (1969).

²¹J. A. Dionne, L. A. Sweatlock, H. A. Atwater, and A. Polman, *Phys. Rev. B* **72**, 075405 (2005).

²²In Refs. 27, 28, 32, and 35, the volume modes are also called PPW (parallel plate waveguide) modes or fast modes.

²³R. W. Wood, *Phil. Mag.* **4**, 396 (1902).

²⁴U. Fano, *J. Opt. Soc. Am.* **31**, 213 (1941).

²⁵A. W. Trivelpiece, *Slow wave propagation in plasma waveguides*, Ph.D. thesis, California Institute of Technology, Pasadena, California (1958).

²⁶A. Oliner and T. Tamir, *J. Appl. Phys.* **33**, 231 (1962).

²⁷A. J. Lichtenberg and J. R. Woodyard, *J. Appl. Phys.* **33**, 1976 (1962).

²⁸C. Davis and T. Tamir, *J. Appl. Phys.* **37**, 461 (1966).

²⁹W. L. Barnes, A. Dereux, and T. Ebbesen, *Nature* **424**, 824 (2003).

- ³⁰E. Ozbay, *Science* **311**, 189 (2006).
- ³¹H. Atwater, *Sci. Am.* **296**, 57 (2007).
- ³²K. Kim, *J. Opt. A: Pure Appl. Opt.* **11**, 075003 (2009).
- ³³S. Kohen, B. Williams, and Q. Hu, *J. Appl. Phys.* **97**, 053106 (2005).
- ³⁴N. W. Ashcroft and N. D. Mermin, *Solid State Physics* (Saunders College, Philadelphia, 1976).
- ³⁵K. Kim, Y. Cho, H. Tae, and J. Lee, *Opt. Express* **14**, 320 (2006).
- ³⁶B. Williams, S. Kumar, H. Callebaut, Q. Hu, and J. Reno, *App. Phys. Lett.* **83**, 5142 (2003).
- ³⁷M. Belkin, J. Fan, S. Hormoz, F. Capasso, S. Khanna, M. Lachab, A. Davies, and E. Linfield, *Opt. Express* **16**, 3242 (2008).
- ³⁸B. Williams, S. Kumar, Q. Hu, and J. Reno, *Opt. Express* **13**, 3331 (2005).
- ³⁹G. R. Parkins, W. E. Lawrence, and R. W. Christy, *Phys. Rev. B* **23**, 6408 (1981).
- ⁴⁰M. Rochat, L. Ajili, H. Willenberg, J. Faist, H. Beere, G. Davies, E. Linfield, and D. Ritchie, *Appl. Phys. Lett.* **81**, 1381 (2002).
- ⁴¹K. Zhang and D. Li, *Electromagnetic Theory for Microwaves and Optoelectronics*, 2nd ed. (Springer, New York, 2007).
- ⁴²L. Landau and E. Lifshitz, *Quantum Mechanics. Non-relativistic Theory*, 3rd ed., Course of Theoretical Physics, Vol. 3 (Pergamon Press, Oxford, 1977).
- ⁴³M. J. Adams, *Introduction to Optical Waveguide* (Wiley, New York, 1981).
- ⁴⁴J. A. Dionne, L. A. Sweatlock, H. A. Atwater, and A. Polman, *Phys. Rev. B* **73**, 035407 (2006).
- ⁴⁵V. Agranovich and V. Kravtsov, *Solid State Commun.* **55**, 85 (1985).
- ⁴⁶V. L. Ginzburg, *The Propagation of Electromagnetic Waves in Plasmas* (Pergamon Press, New York, 1970).
- ⁴⁷M. Born and H. Kun, *Dynamical Theory of Crystal Lattices* (Clarendon Press, Oxford, 1954).
- ⁴⁸B. Williams, *Nature Photonics* **1**, 517 (2007).
- ⁴⁹A. Hugi, R. Maulini, and J. Faist, *Semicond. Sci. Technol.* **25**, 083001 (2010).
- ⁵⁰A. Wittmann, T. Gresch, E. Gini, L. Hvozdar, N. Hoyler, M. Giovannini, and J. Faist, *IEEE J. Quantum Electron.* **44**, 36 (2008).
- ⁵¹A. Lyakh, R. Maulini, A. Tsekoun, R. Go, and C. K. N. Patel, *Appl. Phys. Lett.* **92**, 211108 (2008).
- ⁵²H. Kogelnik and C. V. Shank, *J. Appl. Phys.* **43**, 2327 (1972).
- ⁵³R. Kazarinov and R. Suris, *Sov. Phys. Semicond.* **6**, 1184 (1973).
- ⁵⁴J. Faist, C. Gmachl, F. Capasso, C. Sirtori, D. Sivco, J. Baillargeon, and A. Cho, *Appl. Phys. Lett.* **70**, 2670 (1997).